

Efficient segmentation technique for noisy frontal view iris images using Fourier spectral density

Niladri B. Puhan · N. Sudha ·
Anirudh Sivaraman Kaushalram

Received: 4 August 2008 / Revised: 27 October 2009 / Accepted: 28 October 2009 / Published online: 25 November 2009
© Springer-Verlag London Limited 2009

Abstract In a less constrained capture of iris images to build a high-speed iris recognition system, the design of a robust and fast iris segmentation method is important. In this paper, a new iris segmentation technique based on the Fourier spectral density is proposed for noisy frontal view eye images captured with minimum cooperation from the subjects. The proposed segmentation method is not an iterative technique and it runs in deterministic time. The computational complexity of the proposed method is found to be significantly lower than the existing approaches based on integro-differential operator, Hough transform and active contour. The basic idea underlying the proposed method is to localize the limbic and pupil boundaries using the Fourier spectral density. The performance studies on a recently created iris database, called UBIRIS (Proenca and Alexandre in *Lect Notes Comput Sci* 3617:970–977, 2005) containing defocused, reflection-contained and eyelid-occluded iris images in visible spectral range, show that the proposed method is much faster than the existing methods and simultaneously achieves good segmentation accuracy.

Keywords Iris recognition · Segmentation · Image · Low complexity · Fourier spectral density

N. B. Puhan · N. Sudha (✉)
School of Computer Engineering, Nanyang Technological
University, Singapore, Singapore
e-mail: sudha@ntu.edu.sg; sudhanatraj@yahoo.com

N. B. Puhan
e-mail: puhan@ntu.edu.sg

A. Sivaraman Kaushalram
Department of Computer Science and Engineering,
Indian Institute of Technology Madras, Chennai, India
e-mail: skanirud@cse.iitm.ac.in

1 Introduction

Security scenario in the twenty-first century has caused the research community from both industry and academia to explore novel methods for automated person authentication and recognition. Biometric techniques such as iris recognition, fingerprinting and face recognition have emerged as effective tools for various security applications in recent times. Iris recognition has received increasing attention due to its uniqueness, stability and non-invasiveness and is expected to provide a promising solution to security in the near future. It has been established that the iris of a human contains an extraordinary texture which is unique to each human being. Recognition of irises captured under less constrained situations (such as acquisition of irises when a person just looks at the camera within a distance and no constraints on the environmental lighting) is challenging due to the following reasons. The applications include fast access control to restricted areas and personal devices such as cell phones, computers and cameras. In the case of personal devices, the built-in cameras taking images in visible spectral range can be used to acquire iris images for person authentication. In these application scenarios, frontal iris images can be captured but the image of the entire iris texture need not be available due to occlusion by the eyelid and other noise factors such as eyelashes and specular reflections. The size and the quality of the iris images may vary based on the camera-to-eye distance and the lighting condition. Preprocessing techniques are necessary to localize and normalize the iris and to enhance the iris image. Suitable feature extraction and matching techniques are necessary to achieve high performance in a reliable iris recognition system.

A typical iris recognition system consists of three steps: (1) segmentation; (2) normalization; and (3) feature extraction and matching. This paper focuses on the segmentation of

iris from the eye image. In the literature, a number of methods have been proposed for iris segmentation. Daugman [1] used an integro-differential operator to find both inner and outer boundaries of the iris. The outer and inner boundaries are commonly referred as limbic and pupil boundaries. The center and radius parameters of these circular boundaries are searched in the three dimensional parametric space to maximize the evaluation functions of the model. Wildes [2] performed edge detection through the gradient-based Canny edge detector followed by circular Hough transform for iris localization. This segmentation approach is widely applied to various iris recognition methods. Ma et al. [3,4] estimated the iris region before performing edge detection and Hough transform. This reduced the search space of Hough transform resulting in a lower computational cost. Recently, Daugman [5] suggested active contours to enhance iris segmentation. He approximated both boundaries in terms of Fourier series expansions (FSE) of the contour data. Another Fourier series based description for pupil shape is given in [6]. Some other active contour based approaches for iris segmentation are described in [7,8]. In [8], geodesic active contours were applied for segmentation in infra-red iris images.

These iris segmentation algorithms achieve high performance on iris database images captured in favorable conditions. The images are collected under constrained environment with good lighting and with subject's cooperation (eyes wide open). In these high quality iris images, various noise factors are minimized by using suitable image acquisition techniques. This situation can happen when the system is used for authentication. However, when user cooperation is not available in high speed recognition for fast access and automatic surveillance, it is not easy to obtain high quality iris images. The images may be blurred due to poor focus and have reflections due to different light sources and spectacles. The iris in the image may also be occluded by eye lids.

Currently, recognition of non-cooperatively captured iris images is receiving special attention in iris recognition research. An iris acquisition system for a less constrained environment is proposed in [9]. It captures irises while a person is walking through a portal with cameras mounted on it. This setup assumes a modest level of cooperation on the part of the subjects: eyes open, looking at the camera, and walking down the center of the portal without exaggerated motions. The system performs an initial coarse segmentation of images to isolate eye images by detecting specific configuration of specular reflections caused by the illuminators. Then Daugman's segmentation and recognition algorithm [1] are applied to these eye images. While most research has been focused on the development of algorithms for frontal view iris images, Stephanie et al. [10] devised techniques for off-angle iris images. The techniques are based on (1) angle

estimation and geometric transformation and (2) angular deformation calibration model. Since the iris boundaries need not be circular for off-angle images, a modification to Daugman's integrodifferential operator was suggested for segmentation of iris.

Recently, a public iris database has been created [11] for evaluating the robustness of iris recognition methods. It provides frontal view eye images with different types of noise such as blurring, occlusion and specular reflections, simulating the acquisition of iris images with minimum cooperation from the subjects. Recognition of these irises simulates the situation in which the iris recognition is performed when a person looks at the camera while moving in a well-lit environment (without any special lighting for eye). Since recognition performance critically depends on the segmentation accuracy, it is necessary to design accurate segmentation methods for noisy iris images. A robust iris segmentation method has been proposed in [12] which has been tested over UBIRIS database. In this method, clustering algorithm is applied to classify the pixels based on proximity and intensity values. The algorithm produces an intermediate image in which the pixels belonging to a cluster have the same intensity. Then an edge detection algorithm is applied on the intermediate image. Finally, circular Hough transform is used on the edge map to detect the iris boundaries. Both the clustering algorithm and the Hough transform are computationally intensive due to their iterative approach. In [12], a comparison study has been conducted to check the performance of existing segmentation methods on UBIRIS database. Though the methods achieve good segmentation accuracy, they are computationally very expensive.

In this paper, we propose a new segmentation method for noisy frontal view iris images using Fourier spectral density and other simple image processing techniques. The method can segment the iris in a few scans on the image. From the experimental studies on UBIRIS database, it is found that the proposed method can achieve good segmentation results on noisy iris images in visible spectral range. The proposed method has the advantage of lower computational complexity as compared to the existing segmentation methods which do segmentation iteratively. To the best of our knowledge, it is the first iris segmentation method that performs segmentation in deterministic time.

The organization of the paper is as follows: Sect. 2 discusses the computational complexity of key techniques in existing segmentation methods and the motivation behind proposing a new method. In Sect. 3, the new segmentation method using the Fourier spectral density is described. In Sect. 4, the performance of the proposed method is demonstrated using the noisy iris images in visible spectral range from UBIRIS database. Section 5 gives a comparison with existing methods in terms of complexity analysis. Finally conclusions are given in Sect. 6.

2 Key techniques in existing methods

The review of the iris recognition techniques in literature reveals two major approaches for iris segmentation: Daugman's integro-differential operator and Hough transform-based. Almost all existing methodologies use one of these two or their variants for segmentation. Recently, active contour based methods have been explored for segmentation. We describe all these methods, their computational complexities and their drawbacks next.

2.1 Integro-differential operator

Daugman used an integro-differential operator for segmenting the circular iris and pupil regions. The integro-differential operator is defined as

$$\max_{(r, x_0, y_0)} \left| G_\sigma(r) * \frac{\partial}{\partial r} \oint_{r, x_0, y_0} \frac{I(x, y)}{2\pi r} ds \right|$$

where $I(x, y)$ is the image, r is the radius to search for, $G_\sigma(r)$ is a Gaussian smoothing function, and s is the contour of the circle given by r, x_0, y_0 . The operator searches for the circular path where there is maximum change in pixel values, by varying the radius r and the center (x, y) of the circular contour. The operator is applied iteratively with the amount of smoothing progressively reduced in order to obtain accurate localization. Though the method is effective on images with high contrast between sclera, iris and pupil regions, it can fail due to localized noise such as specular reflections. This method has the computational complexity in the order of $[X \times Y \times R]$ steps for computing the circle parameters where, X and Y are the number of values in the x and y ranges for the center coordinate and R is the number of values in the range for radius. Thus a total of R scans are necessary to compute the circle parameters using this approach.

2.2 Hough transform

The Hough transform is an image processing technique which is effective in determining the parameters of simple geometric shapes such as lines and circles. The circular Hough transformation is applied to compute the radius and center coordinates of the circular iris and pupil regions. In iris segmentation, an edge map is created by computing the first derivatives of intensity values in an iris image and then performing thresholding on the result. Then Hough transformation is applied for computing the parameters of circles passing through each edge point. The parameters such as the center coordinates (x_c, y_c) and the radius r , define a circle according to the following equation

$$(x - x_c)^2 + (y - y_c)^2 = r^2$$

The Hough transform works on the binary edge map as follows for iris segmentation to compute these parameters.

1. Let the number of edge pixels be N_{edge} . A three dimensional accumulator array is created with discrete values of x and y coordinates of the circle center and the radius r . Let R be the range of radius values, X and Y be the ranges of x - and y -coordinate values of the center of the circle.
2. The three dimensional array is scanned using x -coordinate and y -coordinate parameters of the center of the circle. The radius parameter is found for an edge pixel after solving for the radius parameter using the equation of the circle. In the accumulator array, the value of that particular element (whose indices correspond to the chosen coordinate values and the rounded value of the radius) is incremented by one.
3. The above procedure (step 2) is repeated for N_{edge} pixels in the edge map. After all the edge pixels have been scanned, the maximum in the accumulator array is found. The whole process requires $(X \cdot Y)$ computations for each of the edge points and hence there are $(N_{\text{edge}} \cdot X \cdot Y)$ computations for the whole image. Thus a total of N_{edge} scans are necessary to compute the circle parameters using the Hough transform.

2.3 Active contours

Active contours enhance iris segmentation, because they allow for non-circular boundaries and enable flexible coordinate system. The contour is especially useful to create a binary mask that eliminates eyelashes and eyelids for matching. In [5], Daugman described the iris inner and outer boundaries in terms of active contours based on discrete FSE of the contour data. By employing Fourier components whose frequencies are integer multiples of $1/(2\pi)$, closure, orthogonality, and completeness are ensured. Selecting the number of frequency components allows control over the degree of smoothness that is imposed and over the fidelity of the approximation.

Suppose $\{r_\theta\}$ for $\theta = 0$ to $\theta = N - 1$ are N regularly spaced angular samples of radial gradient edge data. The FSE method starts by calculating M discrete Fourier coefficients $\{C_k\}$ of data sequence $\{r_\theta\}$. From these M coefficients, the iris boundary is approximated with N new edge points as

$$R_\theta = \frac{1}{N} \sum_{k=0}^{M-1} C_k e^{j2\pi k\theta/N}$$

In this Fourier series approximation of iris boundaries, the edge pixels of iris boundaries are assumed to be available.

Geodesic active contours in [8] use the level set representation of an active contour. The active contour is given by

a parametric curve $\gamma(t)$. The level set representation of the contour is a 2D function $\psi(x, y)$ that specifies the closest distance of a given point (x, y) to the parametric curve $\gamma(t)$. Thus, the set of points where ψ is zero correspond to the active contour. Unlike conventional approaches where γ is evolved to its final position, the function ψ is evolved in the geodesic approach. The evolution happens under the action of image forces such as gradients (that represent edges) and internal forces that enforce a certain degree of smoothness on the evolving contour. In [8], the pupil boundary is first detected. The initial curve is assumed to be a circle of radius r just beyond the papillary boundary. It is then evolved till it fits the outer boundary of the visible iris region. The equation for evolution of ψ is given by

$$\psi_t = -K(c + \varepsilon\kappa)|\nabla\psi| + \nabla\psi\nabla K$$

where K is the stopping term for the evolution, c is the velocity of evolution, ε indicates the degree of smoothness of the level sets and κ is the curvature of the level sets. The stopping function K is an edge map and its goal is to slow down the evolution when the iris boundary is reached. κ is expressed in terms of first and second order gradients of the image in x and y directions. The extracted contour is then used to estimate the circles to fit the boundaries of iris.

The different steps in obtaining the active contour in [8] are:

1. Preprocessing such as median filtering, minimum finding and thresholding which are performed in three image scans.
2. Circle fitting to detect the pupil boundary from the pre-processed image which takes N_{CF} scans.
3. Edge detection for K which takes one scan on image.
4. Evolution of initial contour that takes N_{step} scans.
5. Fitting a circle for iris outer boundary using extracted active contour in a scan.

The method hence takes $N_{CF} + N_{step} + 5$ scans.

2.4 Drawbacks

Most of the existing segmentation methods use preprocessing techniques such as thresholding, clustering and histogram equalization to enhance the quality of the image or to create an edge map. Then they use either integro-differential operator or Hough transform to compute the circle parameters. As the integro-differential operator and Hough transform are computationally intensive due to their ‘brute-force’ approach, the existing methods may not be suitable for high-speed and real-time applications. Though the methods achieve high accuracy in non-cooperative iris recognition scenario [12], their high computational complexity remains

an issue. In the case of Daugman’s active contour-based segmentation [5], edge data of iris boundaries are assumed to be available. Identifying the edge pixels of boundaries is itself a challenging task. In geodesic contour [8], a lot of parameter values have to be chosen and appropriate convergence conditions need to be specified in order to get a well-fitted curve. The parameter values determine the segmentation accuracy. In active contour-based methods, the pupil boundary is detected first. However the boundary between pupil and iris may not be clear in visible spectral range images unlike infrared images. Moreover, these active contour-based methods are iterative techniques like other two methods, and the time taken for convergence and the segmentation accuracy depend on various parameters.

Considering the real-time processing requirements in non-cooperative iris recognition, we propose a new segmentation method to achieve low computational complexity on visible spectral range iris images. The basic idea underlying the new segmentation method is that the partial limbic boundary and the pupil boundary can be localized using the Fourier spectral density of the iris image. The search space for the computation of circle parameters are significantly reduced after localization of the partial boundary.

3 Proposed iris segmentation method

The proposed segmentation method computes the limbic and the pupil boundaries as follows.

3.1 Limbic boundary computation

The following are different steps in computing the limbic boundary.

3.1.1 Binarize by computing Fourier spectral density

For a given gray iris image I , the method begins with the computation of Fourier spectral density (E_F) for an image pixel $I(j, k)$ according to following equation

$$E_F = \sum_{u=0}^{2d} \sum_{v=0}^{2d} |F(u, v)|^2 \quad (1)$$

where $F(u, v)$ is obtained after two-dimensional discrete Fourier transform of the image block $I(j-d : j+d, k-d : k+d)$ and d determines the size of the neighborhood. An appropriate value for d can be chosen empirically by observing the discrimination ability for various values of d . The Fourier spectral density computed for a pixel indicates the energy level in its neighborhood. In an iris image, the energy level at pixels in sclera region is higher than the iris pixels due to the white sclera region. Thus it is possible to

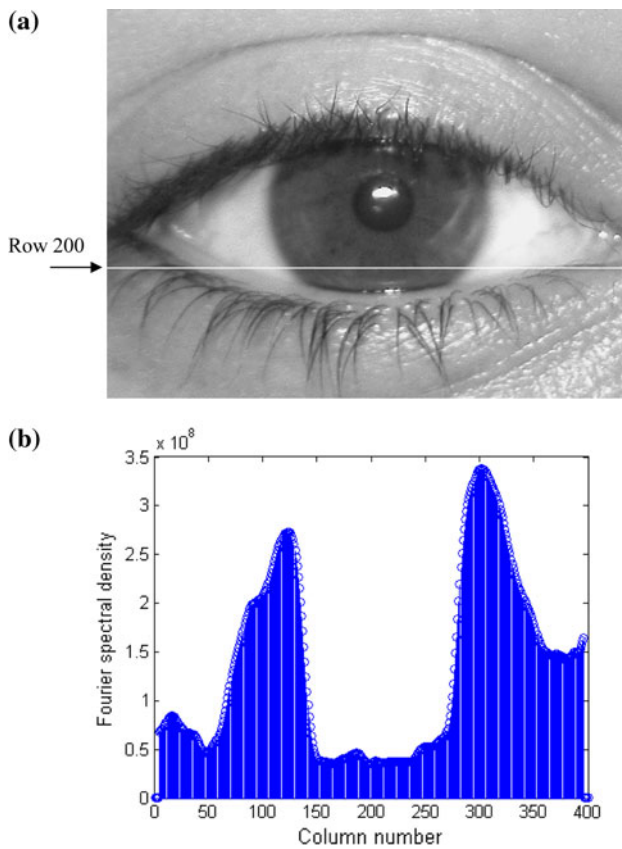


Fig. 1 **a** The iris image of size 300×400 pixels, **b** The Fourier spectral density (E_F) distribution is shown for the pixels at row 200 passing through the iris region

discriminate the sclera and iris region using the Fourier spectral density. Since the neighborhood cannot be defined for the pixels belonging to first d rows and columns as well as last four rows and columns, E_F is not computed in this case. In Fig. 1, the Fourier spectral density distribution (for $d = 4$) is shown for a row of pixels passing through the iris region for an iris image of size 300×400 pixels. It is observed that the peaks in both sides of the distribution correspond to the sclera region pixels while the valley in the middle corresponds to the iris region. We define a binary image I_1 using row-wise adaptive thresholding based on the Fourier spectral density,

$$I_1(j, k) = \begin{cases} 0 & \text{if } E_F \leq E_{th}^{row} \\ 1 & \text{otherwise} \end{cases} \quad (2)$$

where E_{th}^{row} is computed by taking the mean value of E_F in each row of pixels. I_1 is shown in Fig. 2. After further processing, I_1 will show the partial limbic boundary.

3.1.2 Removing specular reflections

In I_1 , there are isolated cluster of white pixels in the iris and pupil regions due to specular reflection and these white pixels are undesirable for segmentation. These white pixels



Fig. 2 The initial binary image (I_1) after thresholding the Fourier spectral density

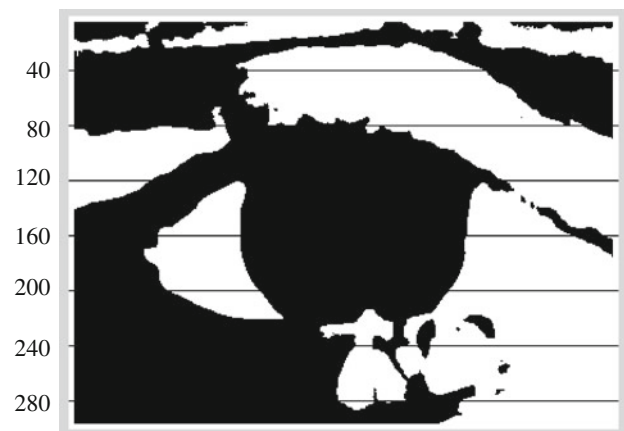


Fig. 3 The image I_1 where isolated clusters of white pixels in iris region are removed after connected component labeling

are removed by performing connected component labeling in the image I_1 . If the number of pixels in a connected component of white pixels is less than a threshold, the component is identified for conversion to black pixels. For a threshold of 1,500 determined empirically, the image in Fig. 3 shows how 11 isolated clusters of white pixels are converted to the black pixels which results in a uniformly black iris and pupil regions.

3.1.3 Localization of partial limbic boundary

For each row j (except the first four and last four rows) in I_1 , find the nearest and farthest white pixels to the first pixel in the row. Let the column numbers of those pixels be denoted by w_n and w_f respectively. The length of largest black pixel sequence (L_b) between the columns w_n and w_f in each row j is found. If w_n and w_f cannot be found when all pixels in the row are black, then L_b is equal to zero. In Fig. 4, L_b is shown corresponding to each row number. From the binary image in Fig. 3, it is observed that the iris is represented by the

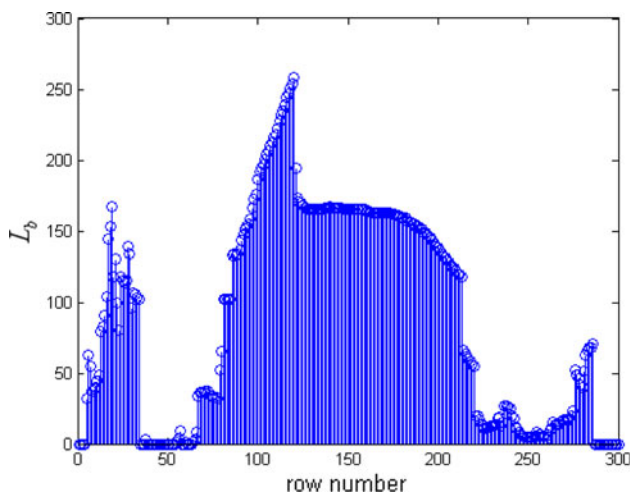


Fig. 4 The length of largest black pixel sequence (L_b) prefixed with a white pixel for each row number

circular black region surrounded by white region representing the sclera. The magnitude of L_b varies smoothly along a certain portion of the iris region due to its circular shape as seen in Fig. 4.

A gradient value (S_g^j) is computed for each row j as follows:

$$\text{gradient} = \begin{cases} |L_b(\text{current row number}) - L_b(\text{previous row number})| \\ + |L_b(\text{current row number}) - L_b(\text{next row number})| & \text{if } (L_b > 50) \\ 0 & \text{otherwise} \end{cases} \quad (3)$$

$$S_g^j = \begin{cases} 1 & \text{gradient} \leq g \\ 0 & \text{otherwise} \end{cases} \quad (4)$$

In the case of typical iris images whose r_1 is around 100 pixels, the condition ($L_b > 50$) holds true for a significant portion of the circular iris region. To illustrate, a circle is shown in Fig. 5a with center ‘O’ and radius r_1 . The chord ‘BD’ of length L_b represents the largest black pixel sequence for the row passing through the circle. From the triangle ‘OBC’, it is evident that

$$OC = \sqrt{r_1^2 - (L_b/2)^2} \quad (5)$$

In Fig. 5b, the magnitude of OC is shown in terms of the percentage of r_1 when a typical r_1 varies from 80 to 120 pixels and $L_b = 50$. The high percentage of OC shows that a significant portion of the circular iris region is captured after using the condition ($L_b > 50$). Using the condition ($L_b > 50$) in Eq. 3, the rows with low value of L_b passing through the non-iris region are eliminated from further processing. The threshold g in Eq. 4 is chosen to take into account only the smooth change in L_b and to avoid changes in L_b due to noise in the iris boundary. In Fig. 6a, the gradient signal (S_g) is shown for $g = 5$. From S_g (which consist of 1’s

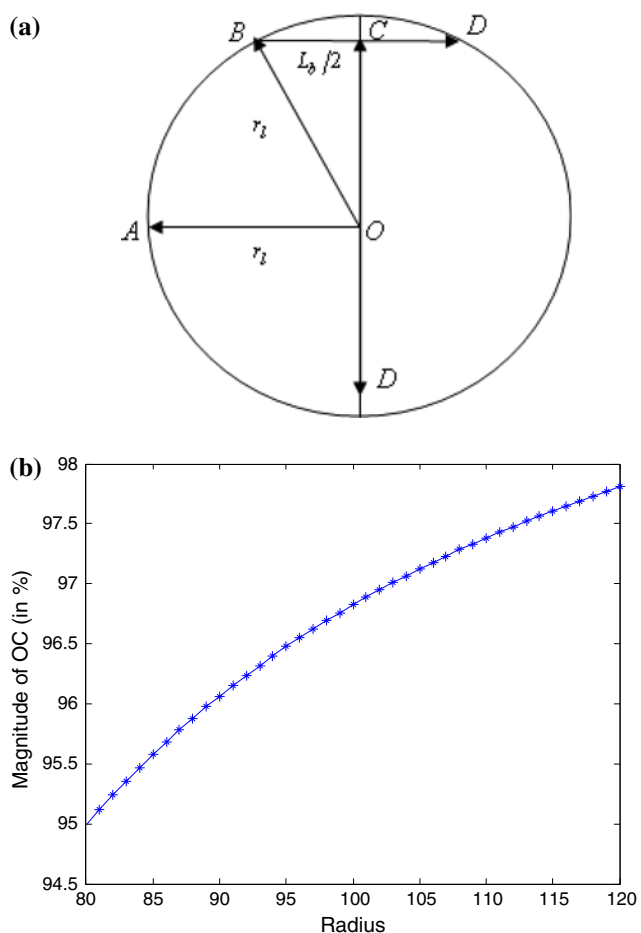


Fig. 5 a A circle is shown with center ‘O’ and radius r_1 , b the magnitude of OC in terms of the percentage of r_1

and 0’s), a final sequence (S_F) containing only the largest sequence of 1’s is found (Fig. 6b).

The final binary image I_c is constructed by considering only the start and end pixels of the largest black pixel sequence for rows corresponding to the sequence of 1’s in S_F (Fig. 7). The black pixels in the binary image represent the partial limbic boundary.

3.1.4 Computing the center and radius parameters

The radius r_1 of the limbic boundary is initialized to

$$r_1 = \begin{cases} \frac{(L_M-1)}{2} & (L_M \text{ is odd}) \\ L_M/2 & (L_M \text{ is even}) \end{cases} \quad (6)$$

where L_M is equal to L_b of the particular row number in S_F for which the gradient value is 1 and L_b is maximum. The starting pixel coordinate of the largest black pixel sequence for this row number is used to compute the center of the limbic boundary. Let the start pixel coordinate for the row

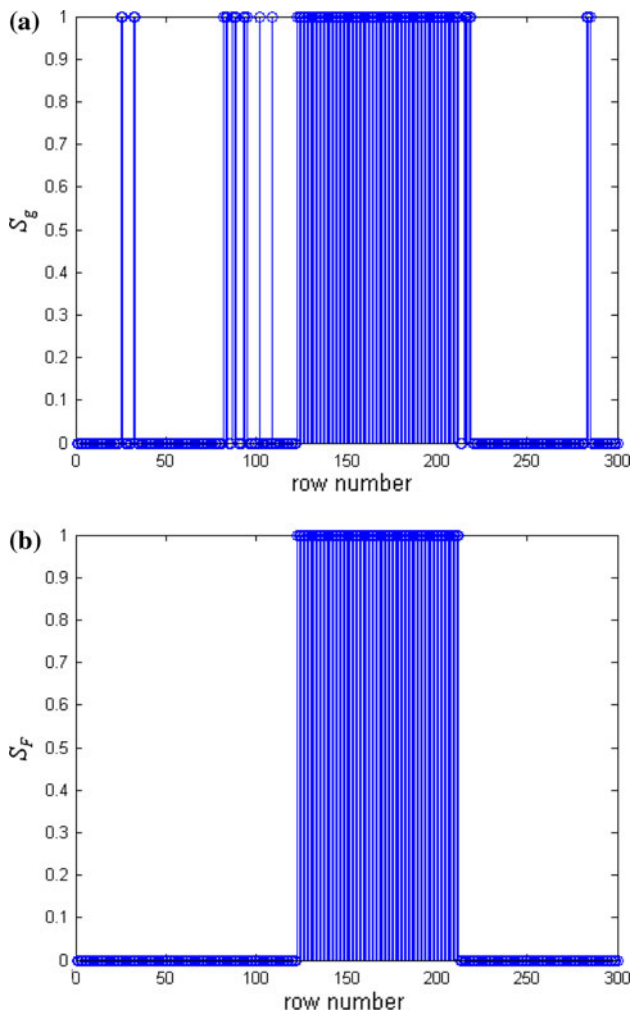


Fig. 6 a The gradient signal (S_g) corresponding to each row, b The final sequence (S_F) containing only the largest sequence of 1's

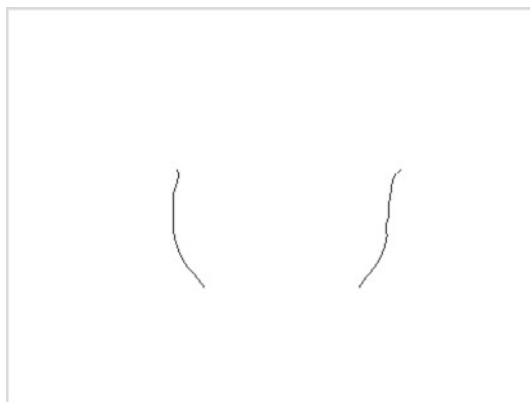


Fig. 7 The final binary image I_c consisting of the start and end pixels of the largest black pixel sequence representing the partial limbic boundary

number is denoted as (j_s, k_s) . The center c_1 of the limbic boundary is initialized to

$$c_1 = [j_s, k_s + r_1] \tag{7}$$

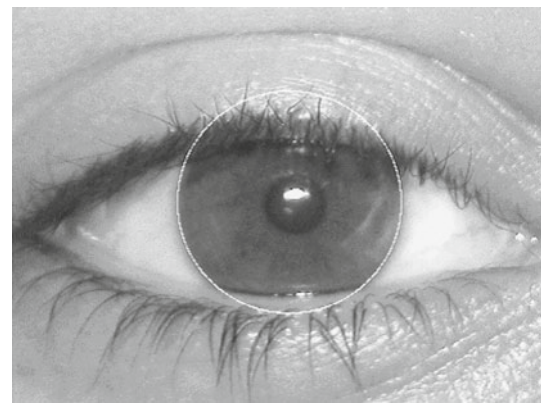


Fig. 8 The image showing the limbic boundary

By using these center and radius values, the actual center and radius of the limbic boundary are computed from I_c . The search for center pixel is first performed in the vertical direction centered at c_1 . Let the pixels considered for searching be the candidate center pixels and they are obtained by changing the row coordinate of c_1 . Given a search range limit n_{row} , the candidate center has a row coordinate in the range $[c_1 - n_{row}, c_1 + n_{row}]$ while the column coordinate remains fixed. Thus a total of $(2 \times n_{row} + 1)$ candidate center pixels are considered for searching. The Euclidean distance between each black pixel and the candidate center pixel is computed. A total of N_c Euclidean distance values $\{D_{euclid}^i, i = 1, \dots, N_c\}$ computed for each candidate center pixel, where N_c is the number of black pixels in I_c . The standard deviation (σ) among N_c Euclidean distance values are computed. The candidate center pixel with minimum σ value is chosen as the intermediate value of c_1 . It is evident from circle geometry that the pixels on the limbic boundary should be at an equal distance from the center pixel. Thus the Euclidean distance values will be similar resulting in minimum standard deviation for the center pixel.

Then the searching is performed in the horizontal direction centered at the updated c_1 . Given a search range limit n_{col} , the candidate center has a column coordinate in the range $[c_1 - n_{col}, c_1 + n_{col}]$ while the row coordinate remains fixed. Similar to the previous procedure, a total of $(2 \times n_{col} + 1)$ number of candidate center pixels are considered for computing the σ values. The candidate center pixel with minimum σ value is the estimated center pixel (c_1) for the limbic boundary. The estimated radius of the limbic boundary is computed from N_c Euclidean distance values corresponding to c_1 . The radius of the limbic boundary is computed as

$$r_1 = \text{round} \left[\frac{1}{N_c} \sum_{i=1}^{N_c} D_{euclid}^i \right] \tag{8}$$

The image showing the limbic boundary is given in Fig. 8.

3.2 Pupil boundary computation

The pupil boundary exists between the pupil and iris. If the circular pupil region can be extracted, then the pupil boundary can be extracted similar to the procedure used for limbic boundary. However, we have observed in the poor quality iris images that the boundary between the pupil and iris is not prominent. A modification to the method proposed for limbic boundary is necessary to detect the pupil boundary. From the iris structure, it is evident that the center of the pupil boundary is close to the center of limbic boundary. In order to estimate the pupil boundary, we consider a square image segment of $w_{\text{pupil}} \times w_{\text{pupil}}$ pixels centered at c_1 . Let the image segment of size $w_{\text{pupil}} \times w_{\text{pupil}}$ pixels be denoted as I_{pupil} . The choice of w_{pupil} is made depending on the image acquisition so that the pupil region is included in I_{pupil} .

3.2.1 Binarize by computing Fourier spectral density

We consider the low frequency Fourier coefficients while computing the Fourier spectral density as the discriminating feature between iris and pupil regions. Similar to limbic boundary detection, we compute the low frequency transform coefficients for pixels in I_{pupil} . The Fourier spectral density is computed as

$$E_F^{\text{low}} = \sum_{u=0}^{d/2} \sum_{v=0}^{d/2} |F(u, v)|^2 + \sum_{u=0}^{d/2} \sum_{v=2d-2}^{2d} |F(u, v)|^2 \quad (9)$$

The reason for considering only these low frequency transform coefficients is to achieve better discrimination ability between the iris and pupil regions. In Fig. 9, E_F^{low} is shown for pixels in I_{pupil} and the valley indicates the pupil boundary. The valley is created due to the lower energy of the pupil region as compared to the iris. A binary image I_p is created after row-wise adaptive thresholding of the pixels in I_{pupil} based on E_F^{low} .

$$I_p = \begin{cases} 0 & \text{if } (E_F^{\text{low}} \leq (1 + \delta)T_{\text{min}}) \text{ and } (E_F^{\text{low}} \leq T_{\text{mean}}) \\ 1 & \text{otherwise} \end{cases} \quad (10)$$

where T_{min} is the minimum value of E_F^{low} in the particular row, T_{mean} is the mean value of E_F^{low} for all pixels in I_{pupil} and δ is a small value in the range (0,0.5). A scaling factor of $(1 + \delta)$ is used with T_{min} to consider the pixels whose E_F^{low} are close to T_{min} . The condition $E_F^{\text{low}} \leq T_{\text{mean}}$ is applied to maximally avoid considering the pixels in the rows which do not pass through the valley. Then I_p is padded with white pixels such that it is of same size as the original image. I_p is shown in Fig. 10. After subsequent processing steps, I_p will show the partial pupil boundary.

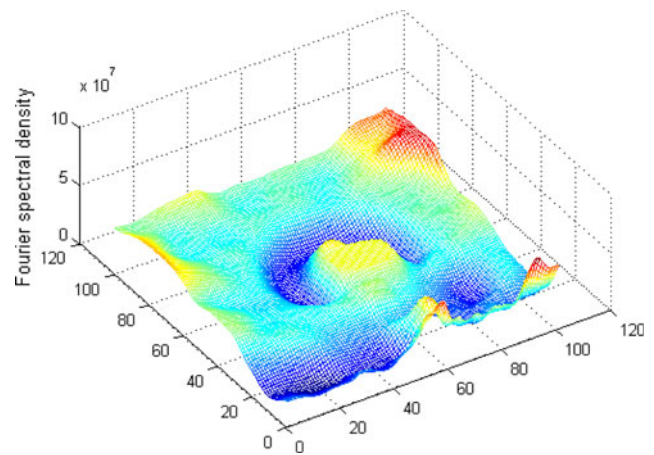


Fig. 9 The Fourier spectral density (E_F^{low}) for pixels in I_{pupil} . The valley represents the pupil boundary



Fig. 10 The initial binary image (I_p) after row-wise adaptive thresholding of the pixels in I_{pupil} based on E_F^{low}

3.2.2 Localization of the pupil boundary

The center for pupil boundary is initialized to c_1 . In I_p , the start and end black pixels of black pixel sequences are computed for each row. The resulting image containing only these start and end black pixels is shown in Fig. 11a. Then the start and end pixels are tested with the initial center of pupil. According to the circle geometry, the center pixel is situated in between the start pixel and the end pixel in a row. The start pixel is retained if its column coordinate is less than the column coordinate of c_1 and the end pixel is retained if its column coordinate is greater than the column coordinate of c_1 . Those start and end pixels in I_p that do not satisfy the conditions are converted to white pixel (Fig. 11b). The start and end pixels within the square image segment of $w_p \times w_p$ pixels centered at c_1 are chosen to represent the iris pupil boundary in I_p . The choice of w_p depends on the radius of the limbic boundary. w_p is much less when compared to the diameter of limbic boundary in most iris images. The image segment of size $w_p \times w_p$ should also accommodate the pupil

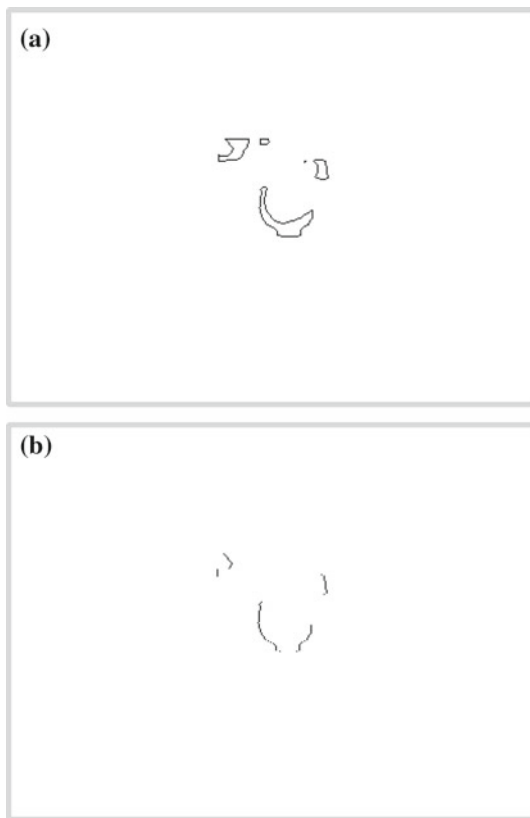


Fig. 11 **a** The intermediate binary image (I_p) containing only the start and end black pixels, **b** the start and end pixels satisfying the circle center conditions in I_p are shown



Fig. 12 The final binary image (I_p) showing the partial pupil boundary

in most iris images. Other pixels outside the square segment in I_p are converted to white pixels. The final I_p showing the partial pupil boundary is displayed in Fig. 12.

3.2.3 Computing center and radius parameters

Given a search range limit n_{pupil} , the search for center pixel for iris pupil boundary is performed in the window of $n_{pupil} \times$

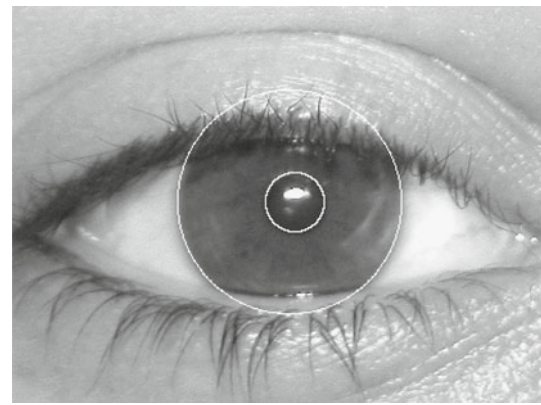


Fig. 13 The image showing both limbic and pupil boundaries

n_{pupil} pixels centered at c_1 . Let the pixels considered for searching be denoted as candidate center pixels. Thus a total of n_{pupil}^2 candidate center pixels are considered for searching. The Euclidean distance between each black pixel and the candidate center pixel is computed. A total of N_p Euclidean distance values $\{D_{euclid}^i, i = 1, \dots, N_p\}$ are computed for each candidate center pixel, where N_p is the number of black pixels in I_p . The standard deviation (σ) among N_p Euclidean distance values is computed. The candidate center pixel with minimum σ value is chosen as the final center pixel c_p for pupil boundary. The radius of the pupil boundary is computed from N_p Euclidean distance values corresponding to c_p . The radius of the pupil boundary is

$$r_p = \text{round} \left[\frac{1}{N_p} \sum_{i=1}^{N_p} D_{euclid}^i \right] \tag{11}$$

The image showing both limbic and pupil boundaries is given in Fig. 13.

3.3 Excluding eyelids and eyelashes

The eyelids and eyelashes normally occlude the upper and lower regions of the iris. To extract the iris pixels not occluded by eyelids and eyelashes, a new method is proposed. The method uses the binary image I_1 in Fig. 3 and the circular limbic boundary in Fig. 8 to exclude the eyelids and eyelashes.

1. Compute edges of binary image I_1 shown in Fig. 3. The edge image is shown in Fig. 14a. The circular limbic boundary is overlapped on it.
2. The edge pixels which are within a small distance from the circular limbic boundary are found out. Figure 14b shows the resulting edge pixels within a Euclidean distance of 5.

3. The edge pixels in a row are removed if any intermediate edge pixel is not connected to the first or last edge pixels. The resulting edge pixels after this operation are shown in Fig. 14c.
4. The first and last edge pixels (F_{edge} and L_{edge}) in the row corresponding to the center of the circular limbic boundary are then identified.
5. A pair of edge pixels (T_{left} and B_{left}) is found using contour tracing [13] beginning at F_{edge} in upward and downward directions respectively. Similarly, another pair of edge pixels (T_{right} and B_{right}) is found using contour tracing that begins at L_{edge} . Figure 14c shows the pixels T_{left} , B_{left} , T_{right} and B_{right} along with F_{edge} and L_{edge} at row 148.
6. A straight line segment connecting T_{left} and T_{right} demarcates the noisy iris region containing upper eyelid and eyelashes. Similarly, another straight line segment connecting B_{left} and B_{right} demarcates the noisy lower region of iris. The line segments are shown in Fig. 14d and the resulting segmented iris is shown in Fig. 14e.

3.4 Computational analysis

To summarize, the proposed method has the following computation steps.

Limbic boundary (1) Fourier spectral density computation, (2) connected component labeling, (3) adaptive thresholding, and (4) computation of N_c Euclidean distances and their standard deviation (σ_c) for a total of $[2 \times (n_{\text{row}} + n_{\text{col}}) + 1]$ pixels. The first three steps create the binary image and the fourth step computes the center and radius parameters.

Pupil boundary (1) computation of E_F^{low} , (2) adaptive thresholding and (3) computation of N_p Euclidean distance values and their standard deviation (σ_p) for a total of n_{pupil}^2 pixels. The first two steps create the binary image and the third step computes the center and radius parameters.

Excluding eyelids and eyelashes (1) computation of the edge image in Fig 14c and (2) contour tracing.

The proposed method is analyzed by finding the number of scans in the image from left to right or from top to bottom. In Fourier spectral density computation, a single scan is performed in the image. For connected component labeling, two scans are required [14] while one image scan is performed for adaptive thresholding. These steps result in four scans. For each edge pixel in I_1 , the computation of Euclidean distances requires $\frac{[2 \times (n_{\text{row}} + n_{\text{col}}) + 1]}{N}$ scan in the image, where N is the number of pixels in the image. Thus for N_c edge pixels, a total of $\frac{N_c \times [2 \times (n_{\text{row}} + n_{\text{col}}) + 1]}{N}$ scans are performed. Similarly in pupil boundary case, the computation of E_F^{low} and

adaptive thresholding requires $\frac{w_{\text{pupil}}^2}{N}$ scan each. For computation of Euclidean distance values, a total of $\frac{N_p \times n_{\text{pupil}}^2}{N}$ scans are performed. For computing the edge image in Fig. 14c, it requires a single scan. The contour tracing step will take N_{trace}/N scans, where N_{trace} is the number of edge pixels in Fig. 14c used in the contour tracing. Thus, the proposed method can compute the center and radius parameters in a total of $\left\{ 4 + \frac{N_c \times [2 \times (n_{\text{row}} + n_{\text{col}}) + 1]}{N} \right\} + \left\{ \frac{2 \times w_{\text{pupil}}^2 + N_p \times n_{\text{pupil}}^2}{N} \right\} + \left\{ 1 + \frac{N_{\text{trace}}}{N} \right\}$ scans where $N_c < N$, $N_p < N$ and $N_{\text{trace}} < N$.

4 Performance evaluation

The performance of the proposed method is evaluated on the UBIRIS eye image database which was created in 2004. The irises in the database simulate the situation in which the iris is captured when a person just looks at the camera in a well-lit environment. The UBIRIS database contains eye images in visible spectral range collected from 241 persons in two distinct sessions. The UBIRIS authors used a Nikon E5700 camera with software version E5700v1.0, 0.71 mm focal length, 4.2 F-Number, 1/30 s exposure time, RGB color representation and ISO-200 ISO speed. The dimension of the captured image is $1,704 \times 2,560$ pixels with 300 dpi horizontal and vertical resolution and 24 bit depth. They were saved in JPEG format with lossless compression. A total of 1,205 images in 241 classes (session 1) and 660 images in 132 classes (session 2) are available. The images in the database are classified with respect to three parameters ('Focus', 'Reflections' and 'Visible Iris') in a three value scale ('Good', 'Average' and 'Bad'). This classification was done manually by UBIRIS authors as: focus (*Good* = 73.83%, *Average* = 17.53%, *Bad* = 8.63%), reflections (*Good* = 58.87%, *Average* = 36.78%, *Bad* = 4.34%) and visible iris (*Good* = 36.73%, *Average* = 47.83%, *Bad* = 15.44%).

The iris test images for the study are chosen from the UBIRIS database because of the heterogeneous image characteristics. They were downsampled to 300×400 in size. Few very bad images in the database are not considered. It is difficult to detect the limbic and pupil boundaries through human observation in 12 images of session 1 and 21 images of session 2. Some of these images are shown in Fig. 15. The reason for difficulty in detecting the boundaries in these images is due to severe occlusion by eyelid or very low contrast between the pupil and iris region. These images are not meaningful to be considered for experimental studies and hence they are removed.

The proposed segmentation method is applied to compute the limbic and pupil boundaries. The different parameters

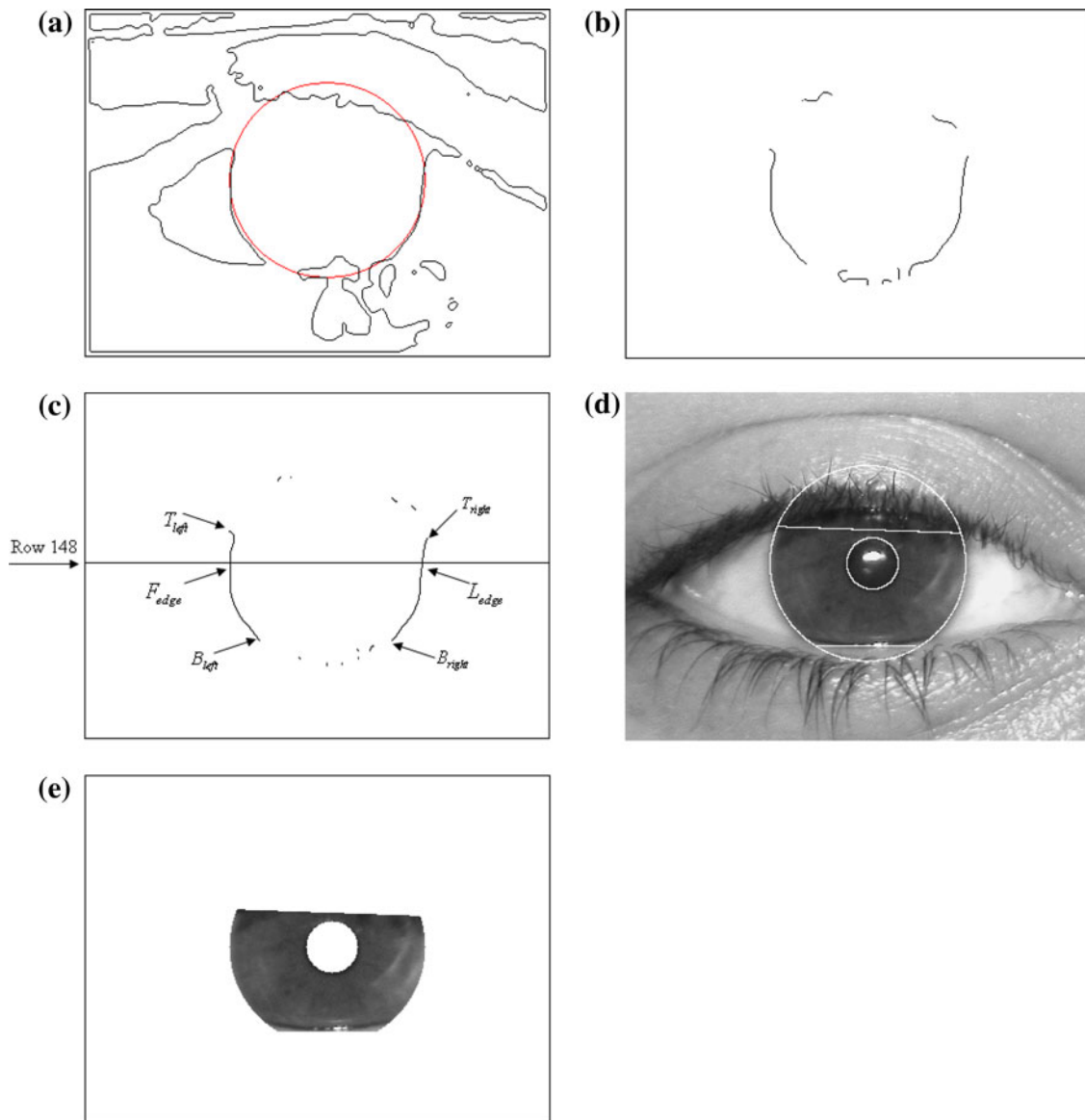


Fig. 14 Exclusion of eyelids and eyelashes

are assigned the values as: $d = 4$; $g = 5$; $n_{\text{row}} = 25$; $n_{\text{col}} = 5$; $w_{\text{pupil}} = 101$; $w_p = 50$; $n_{\text{pupil}} = 21$; $\delta = 0.2$. We decide a correct segmentation in the iris image when the limbic and pupil boundaries obtained through the method match with the ones through human observation. Examples of correct and incorrect iris segmentation are given in Figs. 16a and 17 respectively. Figure 16b shows the segmentation results after excluding eyelids and eyelashes. The segmentation accuracies for limbic boundary in sessions 1 and 2 are found to be 98.49 and 98.75% respectively. The accuracies for the pupil boundary in sessions 1 and 2 are found to be at 94.47 and 87.17% respectively. The low segmentation accuracy for pupil boundary in session 2 images is because the

contrast between the iris and pupil region in noisy images is not prominent even by human observation. However, the limbic boundary detection is very important for many iris recognition methods.

5 Comparison studies

The segmentation accuracies and the computational complexities for the proposed and existing methods are presented in Table 1. The segmentation accuracy results for methods 1–6 for UBIRIS database are obtained from [12]. The result for method 7 is obtained by implementing the technique in [8].



Fig. 15 Examples of very bad category iris images where it is difficult to detect the limbic and pupil boundaries even by human observation

From the table, it is observed that the segmentation accuracy of the proposed method is quite high and is comparable with the existing methods. The computational complexities of the existing methods are presented in terms of number of scans for an image. From the review, the existing methods in Table 1 can be divided into two groups. Methods 1, 2 and 3 use the integro-differential operator. Methods 4, 5 and 6 use the Hough transform after generating an edge map while method 7 is based on geodesic active contour. The complexity of the methods 1, 2 and 3 is same as the integro-differential technique which is R scans in the image, where R is the range of radius values. The value of R is different for limbic and pupil boundaries which are denoted as R^{limbic} and R^{pupil} .

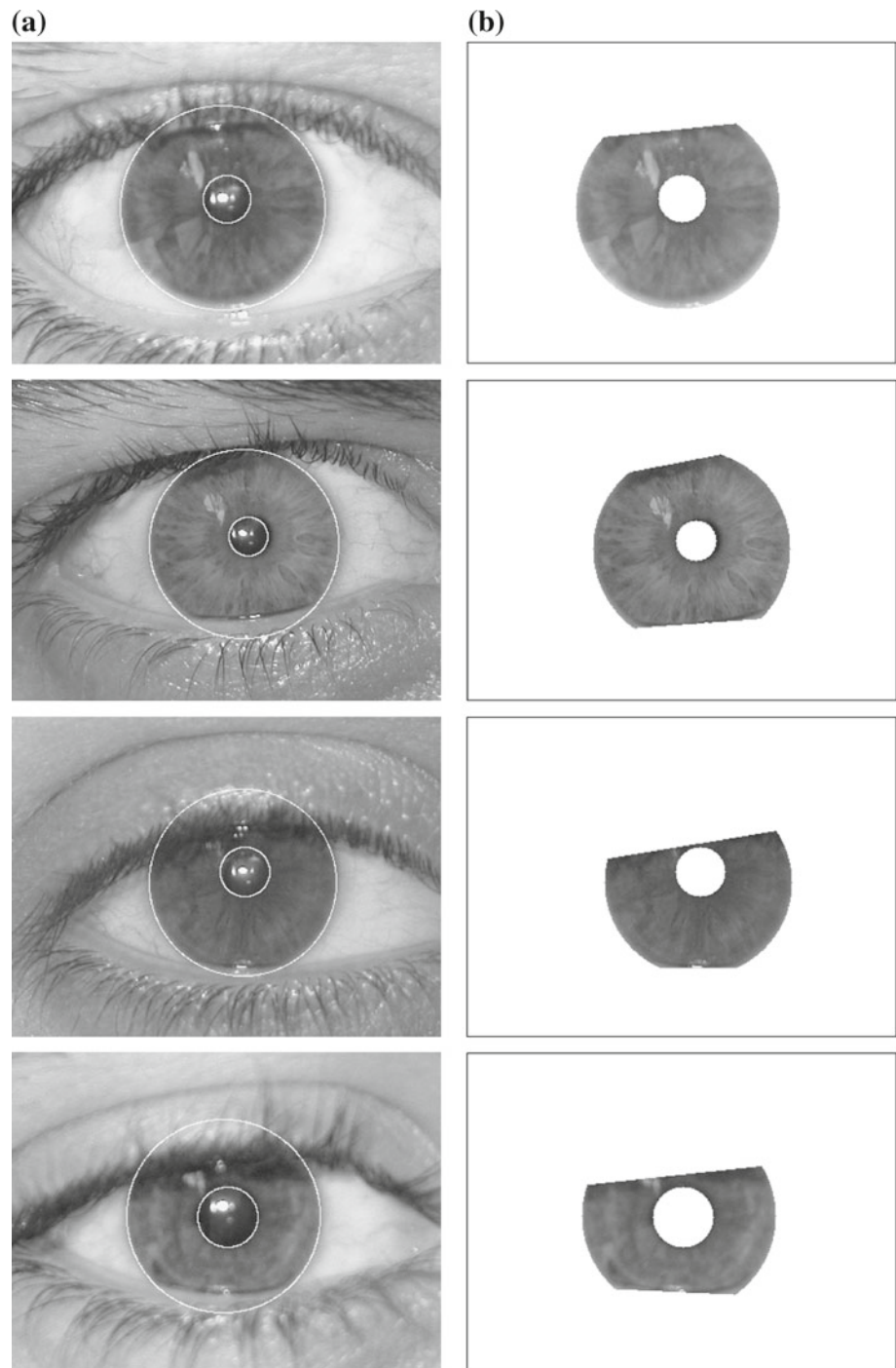
The methods 4, 5 and 6 use different techniques to generate the edge map and the Hough transform is then applied to compute the circle parameters. In method 4, the edge map is constructed by using the Canny edge detector which requires a single scan for computation. In method 5, the K -means clustering technique is applied after computing the moment features at each pixel of the image. The computation of moment features requires a single scan. In method 6, the feature used for K -means clustering is not computed and it is available from image intensity and pixel position. Method 6 also applies K -means clustering. Here, the features are not computed but available from the intensities and the

positions of the pixels. The K -means clustering is an iterative technique that segments the image in several iterations, say K_I , using a distance measure as an evaluation criterion. For clustering operation, K_I scans are necessary. The Hough transform requires N_{edge} scans each to compute the circle parameters for limbic and pupil boundaries. The number of scans taken by method 7 is $N_{\text{CF}} + N_{\text{step}} + 5$ as derived in Sect. 2.3.

For the image in Fig. 1, the number of image scans is computed as follows for different methods. Assume that the radius of limbic boundary varies from 80 to 120 pixels and the radius of pupil boundary varies from 10 to 30 pixels in UBIRIS images. So the complexity of methods 1, 2 and 3 using the integro-differential operator is about 60 scans of the image. For method 4, we computed the edge map of the test image using the Canny operator. The gradients in the operator were biased for vertical direction during the edge detection as suggested by Wildes [2]. The number of edge pixels is found to be 3848. The number of scans for detecting a circle using the Hough transform is same as the number of edge pixels. The K -means clustering operation in the test image takes about 131 scans to isolate the iris region. The number of edge pixels in the edge map generated from the clustered image is 2611. For the proposed method, the value of N_c is equal to 180 pixels while the value of N_p is equal to 40 pixels. The total number of scans for the proposed method is computed to be 5.4. In our implementation of active contour based method [8], we have set different parameters as follows: $c = 0.65$; $\varepsilon = 1$. We applied the Hough transform for fitting circle for the pupil boundary in the preprocessed binary image. N_{CF} is 322 for the test image since the number of feature pixels in the binary image is 322 for a threshold set to 10 during preprocessing. The average number of feature pixels for the UBIRIS database is 356. N_{step} was set to 10. Table 1 gives the average number of image scans and average execution time taken by different methods for the well-segmented images in the UBIRIS database. We have implemented the algorithms in Matlab and executed them on a 2.66 GHz PC running Windows XP and with Pentium 4 processor and 2 GB RAM. It is found that the proposed method takes the least time for segmentation.

The proposed method computes the circle parameters in a few image scans in contrast to the iterative techniques employed in the existing methods. The number of computation steps is significantly low due to the localization of partial limbic and pupil boundaries. The segmentation accuracy is much better when compared to active contours. Though active contours provide a good mask for segmentation, the estimation of circular boundaries of irises using them does not perform well in visible spectral range images. The proposed method is faster and more accurate in locating the iris boundaries.

Fig. 16 Examples of correct segmentation



6 Conclusion

A new segmentation method for noisy frontal view iris images based on the Fourier spectral density has been proposed in this paper. The method computes the Fourier spectral density for each pixel using its neighborhood and then performs row-wise adaptive thresholding which results in a binary image giving the iris region approximately. Further image processing operations on the binary image could compute

the circle parameters for the limbic and pupil boundaries in deterministic time. From the experimental results of testing on the UBIRIS iris database containing visible spectral range iris images, the new method is found to achieve good performance in iris segmentation. The proposed method has significantly lower computations as compared to the existing methods based on integro-differential operator, Hough transform and active contour, and is well suitable for iris recognition in real-time. The recognition system has wide

Fig. 17 Examples of incorrect segmentation

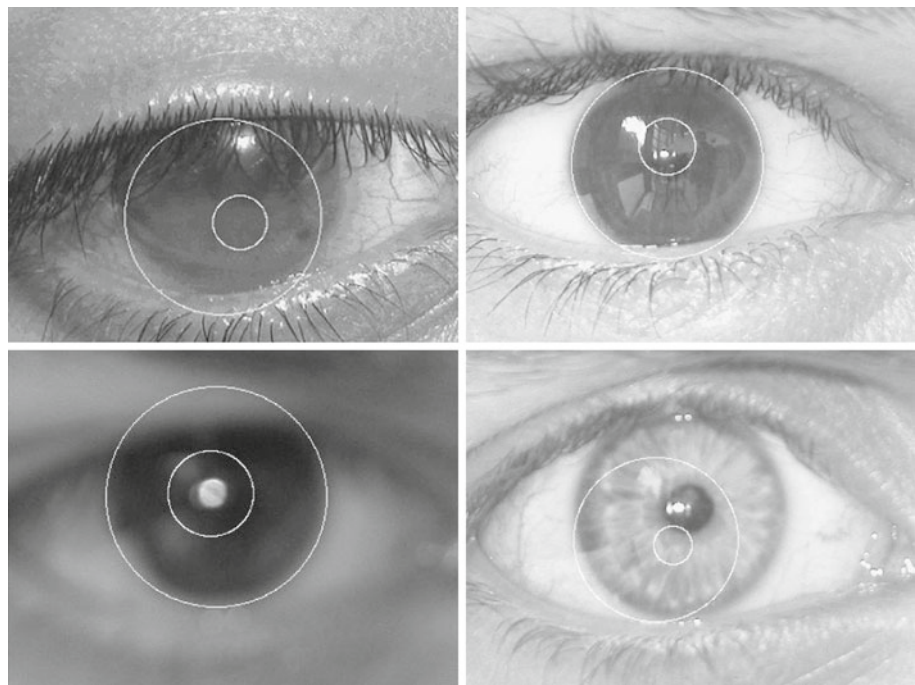


Table 1 Segmentation accuracy and complexity

Methodology	Session 1 (in %)	Session 2 (in %)	Average number of image scans	Average execution time (s)
Daugman [1]	95.22	88.23	$R^{\text{limbic}} + R^{\text{pupil}}$ [60 scans]	39
Camus and Wildes [15]	96.78	89.29	$R^{\text{limbic}} + R^{\text{pupil}}$ [60 scans]	40
Martin-Roche et al. [16]	77.18	71.19	$R^{\text{limbic}} + R^{\text{pupil}}$ [60 scans]	40
Wildes [2]	98.68	96.68	$1 + (2 \times N_{\text{edge}})$ [8,947 scans]	150
Tuceryan [17]	90.28	86.72	$1 + K_I + (2 \times N_{\text{edge}})$ [6,512 scans]	142
Proenca and Alexandre [12]	98.02	97.88	$K_I + (2 \times N_{\text{edge}})$ [6,511 scans]	142
Arun Ross and Samir Shah [8]	67.89	–	$N_{\text{CF}} + N_{\text{step}} + 5$ [371 scans]	25
Proposed method	98.49 (limbic)	98.75 (limbic)	$\left\{ 4 + \frac{N_c \times [2 \times (n_{\text{row}} + n_{\text{col}}) + 1]}{N} \right\}$	15
	94.47 (pupil)	87.17 (pupil)	$+ \left\{ \frac{2 \times w_{\text{pupil}}^2 + N_p \times n_{\text{pupil}}^2}{N} \right\}$	
			$+ \left\{ 1 + \frac{N_{\text{trace}}}{N} \right\}$ [5.4 scans]	

applications in fast identity verification for access control to personal devices and buildings. In access control to buildings, the iris recognition can be performed when a person looks at the camera while moving.

Acknowledgments This work has been supported by the research grant 2006ICTG02 funded by Infocomm research cluster of Nanyang Technological University, Singapore.

References

1. Daugman, J.: High confidence visual recognition of persons by a test of statistical independence. *IEEE Trans. Pattern Anal. Mach. Intell.* **15**(11), 1148–1161 (1993)
2. Wildes, R.: Iris recognition: an emerging biometric technology. *Proc. IEEE* **85**, 1348–1363 (1997)
3. Ma, L., Tan, T., Wang, Y., Zhang, D.: Personal identification based on iris texture analysis. *IEEE Trans. Pattern Anal. Mach. Intell.* **25**(12), 1519–1533 (2003)
4. Ma, L., Tan, T., Wang, Y., Zhang, D.: Efficient iris recognition by characterizing key local variations. *IEEE Trans. Image Process.* **13**(6), 739–750 (2004)
5. Daugman, J.: New methods in iris recognition. *IEEE Trans. Syst. Man Cybern. Part B: Cybern.* **37**(5), 1167–1175 (2007)
6. Rakshit, S., Monroe, D.M.: Pupil shape description using Fourier series. In: *Proceedings of the IEEE Workshop on Signal Processing Applications for Public Security and Forensics*, pp. 1–4 (2007)
7. Arvacheh, E.M., Tizhoosh, H.R.: Iris segmentation: detecting pupil, limbus and eyelids. In: *Proceedings of the IEEE International Conference on Image Processing*, pp. 2453–2456 (2006)

8. Ross, A., Shah, S.: Segmenting non-ideal irises using geodesic active contours. In: Proceedings of the IEEE Symposium on Biometrics (2006)
9. James, R.M., et al.: Iris on the move: acquisition of images for iris recognition in less constrained environments. *Proc. IEEE* **94**(11), 1936–1947 (2006)
10. Stephanie A.C.S., et al.: On techniques for angle compensation in nonideal iris recognition. *IEEE Trans. Syst. Man Cybern. Part B: Cybern* **37**(5), 1176–1190 (2007)
11. Proenca, H., Alexandre, L.A.: UBIRIS: a noisy iris image database. *Lect. Notes Comput. Sci.* **3617**, 970–977 (2005)
12. Proenca, H., Alexandre, L.A.: Iris segmentation methodology for non-cooperative recognition. *IEE Proc. Vis. Image Signal Process.* **153**(2), 199–205 (2006)
13. Pavlidis, T.: Algorithms for Graphics and Image Processing. Computer Science Press, Rockville (1982)
14. Gonzalez, R.C., Woods, R.E.: Digital Image Processing, 2nd edn. Prentice-Hall, Englewood Cliffs
15. Camus, T., Wildes, R.: Reliable and fast eye finding in close-up images. In: Proceedings of the 16th International Conference on Pattern Recognition, pp. 389–394 (2002)
16. Martin-Roche, D., Sanchez-Avila, C., Sanchez-Reillo, R.: Iris recognition for biometric identification using dyadic wavelet transform zero-crossing. *IEEE Aerosp. Electron. Syst. Mag.* **17**(10), 3–6 (2002)
17. Tuceryan, M.: Moment based texture segmentation. *Pattern Recognit. Lett.* **15**, 659–668 (1994)